

Characterization of Steam Generator Tube Deposits and Its Utilization for Chemical Cleaning Process and Corrosion Problems

Soon-Hyeok Jeon, Do Haeng Hur*

Nuclear Materials Research Division, Korea Atomic Energy Research Institute, 989-111, Daedeok-daero,
Yuseong-gu, Daejeon, 34057, Republic of Korea

*Corresponding author: dhhur@kaeri.re.kr

1. Introduction

Corrosion products are released from the surface of the feedwater, condensate, and drain systems. These corrosion products are then transported into the secondary side of a steam generator (SG) in a pressurized water reactor (PWR). Consequently, the corrosion products are deposited on the outer surface of SG tubes and tube sheet in the secondary side of the SG [1,2].

When water is vaporized within the corrosion products deposited on the outer surface of SG tubes, high concentrations of impurities such as chloride, sulfate, and lead are accumulated on the surface of SG tubes, thus forming localized corrosive sites on the tubes [1]. The corrosion products also can decrease the heat transfer efficiency and disrupt thermal hydraulics, [2]. These problems are greatly affected by the physical and chemical properties and quantity of the corrosion products accumulated on the surface of the SG tubes and tube sheet [3]. Therefore, periodic sampling and characterization of SG deposits is very crucial for maintaining the integrity of the SGs.

There are several investigations on the characteristics of the SG deposits in nuclear power plants [4-6]. Tapping et al. [4] performed the detailed analyses of corrosion products in Crystal River Unit 3 SGs and proposed a deposition mechanism of the corrosion products. The Electric Power Research Institute (EPRI) report showed an overview of the characteristics of corrosion products that cause the secondary side problems such as fouling and corrosion [5]. EPRI recently have provided the information on the new technology utilized to collect and characterize SG deposits, which serves as an update and supplement to the EPRI report of 1996 [6]. However, detailed characterization of SG tube deposits according to the position has not been investigated.

In this study, SG tube deposit samples were divided into the three regions by location: 1) water side: a region directly exposed to high-temperature water of the SG, 2) tube side: a region in contact with the outer surface of the SG tube, 3) middle side: an intermediate region between the water and tube sides. The objective of this study is to provide the detailed information of SG tube deposits collected from an operating SG of PWR by using various analysis tools. Based on the results, useful information for corrosion problems and

maintenance actions of SGs such as chemical cleaning process is discussed.

2. Methods

2.1. Materials and elemental analysis

SG tube deposit samples were taken from the outer surface of SG tubes after Cycle 27 during sludge lancing. SG model is Westinghouse model-F. The material of SG heat exchanger tubes from which the deposits samples were collected is Alloy 600TT. The samples obtained from lancing were dried and stored in an airtight container. The elemental composition of the deposit samples was analyzed by induced coupled plasma atomic emission spectroscopy (ICP-AES) and X-ray fluorescence (XRF) spectrometry.

2.2. Porosity analysis

The porosity and pore size distribution of the deposits were measured using cross-sectional scanning electron microscope (SEM) images of the samples in three regions (water, middle, and tube side), which were obtained using an image analyzer. In addition, mercury intrusion porosimetry (MIP) was performed using a penetrometer to determine the pore size in the range from 3 nm to 360 μm . The relation between the pressure p (MPa) and the pore diameter d (μm) could be expressed by Washburn's equation [7], which is based on a model of cylindrical pores. From the Washburn's equation, the relationship between the applied pressure and pore size could be derived. The total porosity and cumulative and differential pore size distribution curve as well as bulk and skeletal densities of the deposit samples could be obtained from MIP results. Bulk density is defined as the weight per unit volume of materials including any interstitial volume and any open or closed pore volume. Skeletal density is calculated after the volume of all the pores has been excluded from the total volume occupied by the materials.

2.3. Microstructural characterization

The morphology of particles on the tube and water sides of the deposits was observed using SEM. The deposit samples were ion-milled using a cross-section polisher in the vertical direction of the samples to measure the thickness of the deposited layer. Then,

cross-sections of the samples were analyzed to observe the pores and measure the thickness of the deposits using SEM.

The cross-sections of the deposits were ion-milled by a focus ion beam (FIB) to prevent the contamination of specimens during sample preparation. The impurity concentration within the pores was analyzed by SEM-EDS analysis of at least five different areas. The phase fraction and grain size of the deposits were analyzed by SEM equipped with an electron back-scatter diffraction (EBSD) pattern analyzer.

3. Results

The elemental composition of the SG tube deposits analyzed using ICP-AES and XRF is presented in Table I. The values are measured with the exception of O. As determined by ICP-AES and XRF data, the main element in the deposits was Fe. Small amounts of Mn, Ni, Cr, Cu, Zn, Ti, Al, Si, and Pb were also detected.

Table I: Elemental analysis of SG tube deposits using ICP-AES and XRF (wt. %).

Element	ICP-AES	XRF
Fe	96.68	93.20
Mn	2.02	2.77
Ni	0.62	2.05
Cr	0.07	0.41
Cu	0.32	0.43
Zn	-	0.37
Ti	0.18	0.40
Al	0.08	0.28
Si	0.03	0.06
Pb	-	0.03

Fig. 1 shows the SEM micrographs of the surface of SG tube deposits on the tube and water sides. The particles on both sides were polyhedral or spherical in shape. Although the particle shapes of both sides were similar, the sizes of particle were greatly different. The tube side of the deposits was composed of very small particles of the size of several tens of nanometers (Fig. 1 (a)). In contrast, the water side of the deposits was consisted of relatively coarse particles, as shown in Fig. 1 (b), and numerous large pores between the particles were also observed.

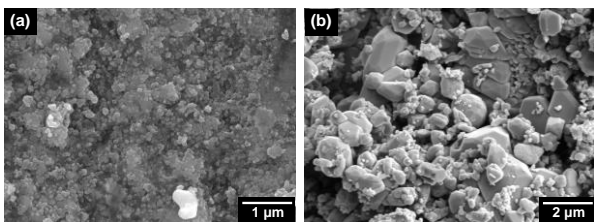


Fig. 1. SEM micrographs of the surface of SG tube deposits: (a) tube side and (b) water side.

Fig. 2 presents the SEM micrograph of the cross-section of the deposits from the tube side to the water side. The cross-section images of the tube side showed a curvature compatible with the outer surface of the SG tube. The thickness of the deposits was about 120 μm. The number and size of the micro-pores observed on the deposits increased from the tube side to the water side. This may be associated with boiling behavior from the tube side to the water side.

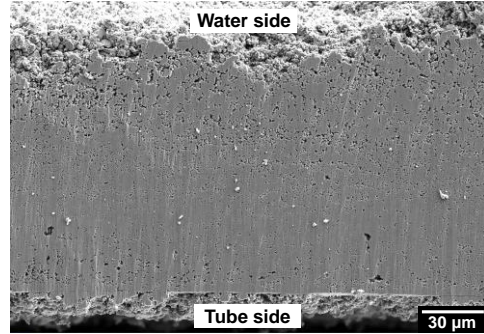


Fig. 2. Cross sectional SEM micrograph of SG tube deposits.

Meanwhile, it is well known that the chemical impurities were predominantly concentrated within the micro-pores formed on the SG tube deposits. Hence, the analysis scope only included the pores, and the chemical composition and concentration of the impurities were analyzed by SEM-EDS mapping. The results are given in Table II. Some impurities such as Na, Cl, P, S, Cu, and Pb were detected within the micro-pores of the deposits.

Table II: Chemical composition of impurities in the pores formed on the tube side of SG tube deposits using SEM-EDS mapping analysis (wt. %).

Element	Tube side
Na	0.02
Cl	0.03 ~ 0.04
P	0.03 ~ 0.04
S	0.03 ~ 0.05
Cu	0.19 ~ 3.13
Pb	0.09 ~ 0.26

Fig. 3 shows the porosity and pore size distribution of the deposits in three different regions calculated using the image analyzer. As shown in Fig. 3 (a), the porosity of the deposits increased from the tube side to the water side. The average porosity of the deposits was about 18 %. The porosity on the water side was approximately 2.5 times higher than that on the tube side. The number of large pores increased from the tube side to the water side (Fig. 3 (b)). The maximum pore diameters on the tube and water sides were about 2.05 μm and 10.35 μm, respectively.

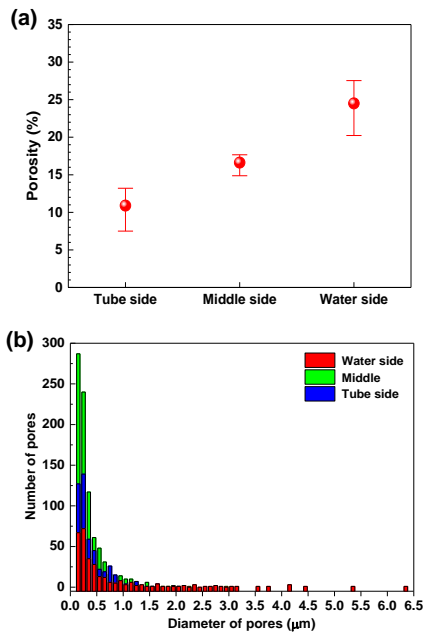


Fig. 3. Porosity analysis of SG tube deposits using image analyzer: (a) porosity and (b) pore size distribution.

Fig. 4 presents the pore size distribution of the deposits measured using MIP. After the measuring the porosity data, the initial cumulative volume by Hg intrusion should be considered the crevices and gaps between the small flake samples because several pieces of samples were packed into a sealed sample cup. Hence, the maximum pore size had to be determined to calculate the porosity of the actual pores within the deposits. The maximum pore diameter for calculation was considered to be about 10 μm according to the results obtained by the image analyzer. After the selection of the maximum pore diameter, porosity of the deposits was calculated using MIP. The porosity and mean pore diameter of the deposits were about 9.82 % and 0.196 μm, respectively. The difference in the mean pore diameter was thought to be due to the micro-pores not being measured by the image analyzer. Furthermore, the bulk and skeletal densities of the samples could be measured by MIP. The bulk and skeletal densities were 2.72 g/cm³ and 3.02 g/cm³, respectively.

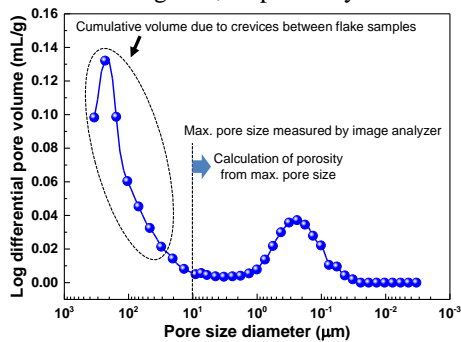


Fig. 4. Pore size distribution of SG tube deposits using MIP.

Fig. 5 shows the 001 IPF orientation and phase distribution map of the deposits for three different

regions. A random orientation was observed in these maps because a predominant color did not appear. The number of grains was decreased from the tube side to the water side. Phases such as magnetite, tremorite, jacobite, and Cu were detected and randomly distributed in all the regions. The deposits were mainly composed of magnetite and contained only small amounts of tremorite, jacobite, and Cu particle.

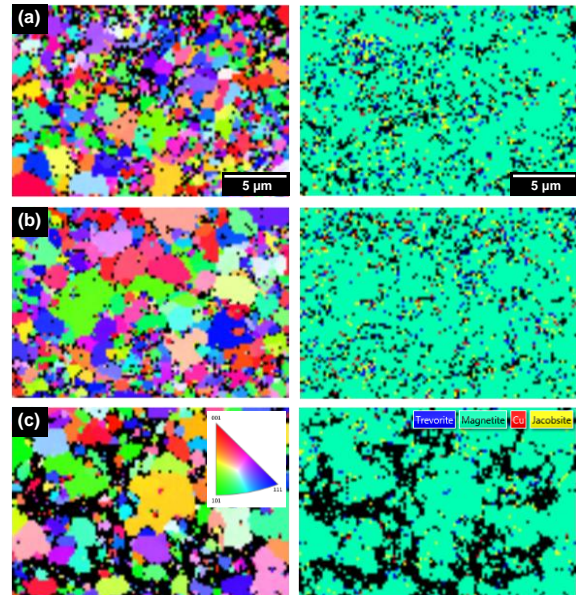


Fig. 5. 001 IPF orientation and phase distribution maps of SG tube deposits using EBSD analysis: (a) tube side, (b) middle side, and (c) water side.

4. Discussion

4.1. Utilization of deposit characterization for chemical cleaning process

The results obtained in this work provide beneficial information for planning chemical cleaning process. First, the results could be used to calculate the total mass of SG tube deposits in a SG to be removed by chemical cleaning process. It is very important to determine the total amount of deposits to optimize the duration and selection of SG maintenance actions such as the chemical cleaning and sludge lancing. In general, if the density and volume of the SG deposits are known, the total mass of the corrosion products deposited on the SG tubes can be calculated. The bulk density of the deposit samples can be obtained using MIP. In addition, assuming that there is no curvature in the SG tubes, the volume of the deposits can be calculated by multiplying the thickness of the deposited layer with the total surface area of the SG tubes. However, it is difficult to calculate exactly the total amount of actual SG tube deposits through this method. Nevertheless, it will be helpful to select the timing and condition of chemical cleaning by calculating the total amount of the deposits.

Second, it could be utilized to calculate the chemical cleaning efficiency. In general, the total amount of

magnetite removed is measured by calculating the concentration of Fe dissolved in the cleaning solution after the chemical cleaning. The cleaning efficiency can be calculated by dividing the total amount of removed magnetite by the magnetite deposited in the SG.

4.2. Utilization for corrosion problems due to the SG tube deposits

The results in this study could be help predict the corrosion behavior of SG tubes. As given in Table II, some impurities such as Na, Cl, P, S, Cu, and Pb are detected in the pores of the SG tube deposits. Each element can cause the corrosion in the SG tubes. For instance, Cu is expected to greatly elevate the electrochemical corrosion potential of the SG tubes and have been associated with many corrosion problems, including stress corrosion cracking (SCC) and localized corrosion of SG tubes [8]. Pb is typically a species of interest in SG tube deposit characterizations because it has been well known to accelerate SCC of nickel-based alloys [8]. S has been associated with intergranular attacks (IGAs) and SCC due to pH effects and with wastage in SG tubes. Furthermore, reduced S has been associated with more severe species-specific corrosion mechanisms, including IGA, pitting corrosion, and SCC [8]. Finally, pitting corrosion is accelerated due to the presence of concentrated Cl in SG tube deposits.

In EPRI guidelines, the concentrations of various impurities in the secondary water of PWRs during operation were limited to mitigate the corrosion problem of SG tubes. The concentration of Cu should be below 1 ppb in a feedwater sample. The concentrations of Na, Cl, and S should be below 5 ppb, 10 ppb, and 10 ppb in a blowdown sample, respectively [8].

So far, many studies have claimed that aggressive impurities are concentrated within the pores of the deposits due to the evaporation of liquid within the micro-pores [1]. However, there is no actual analyzed data or evidence for the concentration of impurities within the micro-pores to support this argument. Hence, the concentration of impurities within the micro-pores of the deposits was analyzed using SEM-EDS mapping analysis (Table II). In addition, the concentration factors of impurities were calculated by comparing with the EPRI guidelines. The concentration factor of Cu within the pores was in the range of $2 \times 10^6 \sim 3 \times 10^7$. For other impurities such as Na, Cl, and S, the concentration factors within the pores were $3 \times 10^4 \sim 5 \times 10^4$. Based on the results, the corrosive environment within the micro-pores and crevices of the deposits could be more precisely predicted.

5. Conclusions

The objective of this study was to characterize the SG tube deposits collected from an operating PWR and

provide useful information for corrosion problems and maintenance actions of SGs. The main conclusions are as follows.

1. The SG tube deposits were mostly composed of magnetite and contained small amounts of trevorite, jacobsonite, and metallic Cu.
2. The porosity and mean pore diameter of the deposits measured by MIP were approximately 9.82 % and 0.196 μm , respectively.
3. The concentration factor of Cu within the pores was in the range of $2 \times 10^6 \sim 3 \times 10^7$. For other impurities such as Na, Cl, and S, the concentration factors within the pores were all included between $3 \times 10^4 \sim 5 \times 10^4$.
4. The density of SG tube deposits was about 2.72 g/cm^3 . This data could be utilized to calculate the total mass of tube deposits in a SG that is to be removed by chemical cleaning. The chemical cleaning efficiency could be also calculated by comparing the total mass of the corrosion products deposited on the SG and the magnetite removed by chemical cleaning process.

ACKNOWLEDGEMENTS

This work was supported by the National Research Foundation of Korea (NRF) grant funded by the Korea government (2017M2A8A4015159).

REFERENCES

- [1] I. H. Plonski, Effect of bare metal surface on the dissolution in aqueous citrate solution of magnetite films on carbon steel, *J. Appl. Electrochem.* 27 (1997) 1184-1192.
- [2] A. A. M. Prince, S. Velmurugan, S. V. Narasimhan, C. Ramesh, N. Murugesan, P. S. Raghavan, R. Gopalan, Dissolution behaviour of magnetite film formed over carbon steel in dilute organic acid media, *J. Nucl. Mater.* 289 (2001) 281-290.
- [3] P. J. Millet, J. M. Fenton, A detailed model of localized concentration processes in porous deposits of SGs. In: Proc. 5th Int. Symp. on Environmental Degradation of Materials in Nuclear Power Systems- Water Reactors. American Nuclear Society, La Grange Park, IL. pp. 745-751.
- [4] R. L. Tapping, C. W. Turner, R. H. Thompson, R. H. Thompson, Steam generator deposits-a detailed analysis and some inferences, *Corrosion* 47 (1991) 489-495.
- [5] EPRI-TR-106048, Characterization of PWR Steam Generator Deposits, EPIR, Palo Alto, CA, USA, 1996.
- [6] EPRI 3002002794, Steam Generator Management Program: PWR Steam Generator Deposit Characterization Sourcebook, EPIR, Palo Alto, CA, USA, 2014.
- [7] E. W. Washburn, Proc. The National Academy of Science, PNASA, pp. 7-21, 1921.
- [8] EPRI 1016555, Pressurized Water Reactor Secondary Water Chemistry Guidelines-Revision 7, EPRI, Palo Alto, CA, USA, 2009.